Channel waveguides and Mach-Zehnder structures on $RbTiOPO_4$ by Cs^+ ion exchange

M. A. Butt,[1] M. C. Pujol,[1] R. Solé,[1] A. Ródenas,[1] G. Lifante,[2] J. S. Wilkinson,[3] M. Aguiló[1] and F. Díaz[1]

[1]*Física i Cristal·lografia de Materials i Nanomaterials (FiCMA-FiCNA) and EMaS, Universitat Rovira i Virgili (URV), Marcel·lí Domingo 1, E-43007, Tarragona, Spain*
[2]*Departamento de Física de Materiales, Universidad Autónoma de Madrid, 28049 Madrid, Spain*
[3]*Optoelectronics Research Centre, University of Southampton, Southampton, SO171BJ, UK*
[4]*mariacinta.pujol@urv.cat*
[5]*rosam.sole@urv.cat*

Abstract: Cs^+ ion exchange in $RbTiOPO_4$ and (Yb,Nb):RTP/RTP(001) has been used to locally increase the refractive indices for waveguide circuit fabrication. Ti masks were fabricated on RTP samples by conventional photolithography. Cs^+ exchange was done using a $CsNO_3$ melt at 698 K during 2 h. Elemental analysis confirms an Cs^+ profile with a variable depth. Apparently the Cs^+ exchange is disfavored in the doped epitaxial sample. The refractive index variation is higher for n_z than for $n_{x,y}$. Near-field images of the guided modes at 633, 1064 and 1520 nm were recorded. The optical characterization shows propagation losses of 5 dB/cm at 1520 nm.

OCIS codes: (130.2790) Guided waves; (130.3130) Integrated optics materials.

References and links

1. P. A. Thomas, S. C. Mayo, and B. E. Watts, "Crystal structures of $RbTiOAsO_4$, $KTiO(P_{0.58},As_{0.42})O_4$, $RbTiOPO_4$ and$(Rb_{0.465},K_{0.535})TiOPO_4$, and analysis of pseudosymmetry in crystals of the $KTiOPO_4$ family," Acta Crystallogr. B **48**(4), 401–407 (1992).
2. M. N. Satyanarayan, A. Deepthy, and H. L. Bhat, "Potassium Titanyl Phosphate and its isomorphs: Growth, properties and applications," Crit. Rev. Solid State Mater. Sci. **24**(2), 103–191 (1999).
3. S. Yu, A. I. Oseledchik, A. L. Pisarevsky, V. V. Prosvirnin, N. V. Starshenko, and N. V. Svitanko, "Nonlinear optical properties of the flux grown $RbTiOPO_4$ crystal," Opt. Mater. **3**(4), 237–242 (1994).
4. Y. Guillien, B. Ménaert, J. P. Féve, P. Segonds, J. Douady, B. Boulanger, and O. Pacaud, "Crystal growth and refined Sellmeier equations over the complete transparency range of $RbTiOPO_4$," Opt. Mater. **22**(2), 155–162 (2003).
5. J. D. Bierlein, D. B. Laubacher, J. B. Brown, and C. J. van der Poel, "Balanced phase matching in segmented $KTiOPO_4$ waveguides," Appl. Phys. Lett. **56**(18), 1725–1727 (1990).
6. G. Lifante, *Integrated Photonics: Fundamentals* (Wiley, 2003).
7. T. Suhara and M. Fujimura, *Waveguide Nonlinear-Optic Devices* (Springer, 2003).
8. T. L. Koch, F. J. Leonberger, and P. G. Suchoski, *Handbook of Optics, Integrated Optics* (McGraw-Hill, 1995).
9. A. Choudhary, J. Cugat, K. Pradeesh, R. Solé, F. Díaz, M. Aguiló, H. M. H. Chong, and D. P. Shepherd, "Single-mode rib waveguides in (Yb,Nb):$RbTiOPO_4$ by reactive ion etching," J. Phys. D **46**(14), 145108 (2013).
10. J. D. Bierlein, A. Ferretti, L. H. Brixner, and W. Y. Hsu, "Fabrication and characterization of optical waveguides in $KTiOPO_4$," Appl. Phys. Lett. **50**(18), 1216–1918 (1987).
11. J. D. Bierlein and H. Vanherzeele, "Potassium titanyl phosphate: properties and new applications," J. Opt. Soc. Am. B **6**(4), 622–633 (1989).
12. M. G. Roelofs, A. Ferretti, and J. D. Bierlein, "Proton-exchanged and ammonium-exchanged waveguides in $KTiOPO_4$," J. Appl. Phys. **73**(8), 3608–3613 (1993).
13. L. Zhang, P. J. Chandler, P. D. Townsend, Z. T. Alwahai, and A. J. McCaffery, "Second-harmonic generation in ion-implanted $KTiOPO_4$ planar waveguides," Electron. Lett. **28**(16), 1478–1480 (1992).
14. N. Yu. Korkishko and V. A. Fedorov, *Ion Exchange in Single Crystals for Integrated Optics and Optoelectronics,* (Cambridge International Science Publishing 1999).
15. M. Roth, *Springer Handbook of Crystal Growth. Stoichiometry and Domain Structure of KTP-Type Nonlinear Optical Crystals,* G. Dhanaraj, K. Byrappa, V. Prasad, M. Dudley, eds. (Springer-Verlag Berlin Heidelberg, 2010), Chapter 20, pp. 691–723.

#234556 - $15.00 USD Received 12 Feb 2015; revised 10 Apr 2015; accepted 11 Apr 2015; published 22 Apr 2015

16. V. D. Kugel, G. Roseman, N. Angert, E. Yaschin, and M. Roth, "Domain inversion in $KTiOPO_4$ crystal near the Curie point," J. Appl. Phys. **76**(8), 4823–4826 (1994).
17. J. Gavaldà, J. J. Carvajal, X. Mateos, M. Aguiló, and F. Díaz, "Dielectric properties of Yb^{3+} and Nb^{5+} doped $RbTiOPO_4$ single crystals," J. Appl. Phys. **111**(3), 034106 (2012).
18. J. Cugat, R. Solé, J. J. Carvajal, X. Mateos, J. Massons, G. Lifante, F. Díaz, and M. Aguiló, "Channel waveguides on $RbTiOPO_4$ by Cs^+ ion exchange," Opt. Lett. **38**(3), 323–325 (2013).
19. P. U. M. Sastry, M. S. Somayazulu, and A. Sequiera, "Influence of some partial substitutions on conductivity and dielectric behaviour of potassium titanyl phosphate," Mater. Res. Bull. **27**(12), 1385–1392 (1992).
20. J. J. Carvajal, M. C. Pujol, and F. Díaz, *Springer Handbook of Crystal Growth. High-Temperature Solution Growth: Application to Laser and Nonlinear Optical Crystals*, G. Dhanaraj, K. Byrappa, V. Prasad, M. Dudley, eds. (Springer-Verlag Berlin Heidelberg, 2010), Chapter 21, pp. 725–757.
21. J. J. Carvajal, V. Nikolov, R. Solé, J. Gavaldà, J. Massons, M. Rico, C. Zaldo, M. Aguiló, and F. Díaz, "Enhancement of Erbium Concentration in $RbTiOPO_4$ by Codoping with Niobium," Chem. Mater. **12**(10), 3171–3180 (2000).
22. J. Cugat, R. M. Solé, J. J. Carvajal, M. C. Pujol, X. Mateos, F. Díaz, and M. Aguiló, "Crystal growth and characterization of $RbTi_{1-x-y}Yb_xNb_yOPO_4$/$RbTiOPO_4$(001) non-linear optical epitaxial layers," CrystEngComm **13**(6), 2015–2022 (2011).
23. Ytterbium and erbium doped $RbTi_{1-x}M_xOPO_4$ (M = Nb or Ta) crystals. New laser and nonlinear bifunctional materials, Alexandra Peña Revellez, Ph. D. Thesis 2007.
24. J. Guo, B. Raghothamachar, M. Dudley, J. J. Carvajal, A. Butt, M. C. Pujol, R. Solé, X. Mateos, J. Massons, M. Aguiló, and F. Díaz, "Effect of doping on crystalline quality of rubidium titanyl phosphate (RTP) crystals grown by the TSSG method," MRS Proceedings, 1698 (2014).
25. V. I. Voronkova, V. K. Yanovskii, T. Yu. Losevskaya, and S. Yu. Stefanovich, "Electrical and nonlinear optical properties of $KTiOPO_4$ single crystals doped by Nb or Sb," J. Appl. Phys. **94**(3), 1954–1958 (2003).
26. A. Peña, B. Ménaert, B. Boulanger, F. Laurell, C. Canalias, V. Pasiskevicius, P. Segonds, C. Félix, J. Debray, and S. Pairis, "Template-growth of periodically domain-structured $KTiOPO_4$ [Invited]," Opt. Mater. Express **1**(2), 185–191 (2011).
27. K. S. Buritskii, E. M. Dianov, V. A. Maslov, V. A. Chernykh, and E. A. Shcherbakov, "Measurement of optical anisotropy in KTP:Rb waveguides," Kvant. Electron. **17**(10), 1369–1370 (1990).
28. K. S. Buritskii, E. M. Dianov, V. A. Maslov, S. Tsygankov, V. A. Chernykh, and E. A. Shcherbakov, "Measurement of optical strength of diffused planar Rb:KTP waveguides," Kvant. Electron. **17**(4), 494–495 (1990).

1. Introduction

$KTiOPO_4$ (KTP) and its isostructural $RbTiOPO_4$ (RTP) are well known crystalline dielectric materials with excellent properties for non-linear optical applications. They crystallize in the noncentrosymmetric orthorhombic space group $Pna2_1$ and for RTP, the unit cell parameters area = 12.974(2)Å, b = 6.494(3)Å and c = 10.564(6)Å [1]. RTP has similar non-linear optical coefficients to KTP [2], a higher laser damage threshold (~2 times larger than that of KTP) [3, 4], a wide range of wavelength and angular acceptance for frequency doubling, high chemical stability, and low photorefractive damage susceptibility [5]. Another important non-linear material is $LiNbO_3$ (LN), which is broadly used for integrated optics (IO) [6, 7]. RTP has a higher damage threshold than LN and similarly large electro-optic coefficients [8]. Both LN and RTP could be used as platform for various IO electro-optical (EO) applications such as modulators and Q-switches. In general, IO devices interface efficiently with optical fibers and can reduce the cost in complex circuits by eliminating the need for separate and individual packaging of each circuit element.

Depending of the refractive index distribution, waveguides (WG) can be classified into two types: graded-index and step-index WGs. Step-index WGs have been fabricated successfully in the RTP crystal by means of reactive ion etching with fluorine chemistry [9]. In the literature, different methods of fabrication of graded-index WG, such as ion exchange [10, 11], proton exchange [12], and ion implantation [13], have been successfully used on KTP.

KTP is a classical ionic conductor, and the vacancy assisted one dimensional ionic conductivity is present. It is known that the ionic conductivity of KTP crystals along the [001] direction is significantly higher than along the other crystallographic directions [14]. The highly anisotropic behavior ensures high aspect ratio with low lateral ion exchange WG, in contrast with LN. Ionic conductivity, directly related to the feasibility of the ion exchange, is

#234556 - $15.00 USD Received 12 Feb 2015; revised 10 Apr 2015; accepted 11 Apr 2015; published 22 Apr 2015

favored by the presence of K^+ vacancies and also affected by the c + or c- surface nature. KTP/ RTP are known ferroelectric materials, with c + and c- domains. For WG preparation in KTP, the ion exchange behavior on the c + surface is different from that on the c- surface. Compared with the c + face, the index change Δn obtained on the c- face is larger, whereas the exchange depth d is smaller [15]. KTP crystals grown from highly concentrated solutions usually crystallize in the paraelectric phase above the Curie temperature, T_c. The ferroelectric domain structure is formed upon post growth cooling, so that the crystals grown with high temperature growth method result in multi domain structures [15, 16].

Literature related to WG with graded-index in RTP is scarce. Even though the Rb^+ ion is larger than the K^+ ion, RTP is also a conventional ionic conductor [17] and vacancy-assisted one dimensional ionic conductivity is also expected. The ionic conductivity of RTP along the [001] direction is lower than that of KTP, but also higher than the ionic conductivity along the other directions [17]. This difference in ionic conductivity between KTP and RTP is due to the different ionic radii of Rb^+ and K^+. The higher ionic radius of Rb^+ contributes to a decrease in its mobility through the channels along the ***c*** direction of the crystal lattice. In any case, the ionic conductivity of RTP along ***c*** direction is high enough to allow Cs^+ exchange into the RTP crystal lattice with concentrations high enough to allow the formation of optical WGs with vertical channel walls parallel to the polar [001] axis. For an ideally controlled ion exchange process it is necessary to know the distribution of c+/c- ferroelectric domains. In RTP, the T_c covers the range from 1043 to 1073 K and the growth temperature used in the TSSG-SC technique in self-flux is usually around 1173 K; so RTP crystals are also obtained in the paraelectric phase. Recently, Cs^+ ion exchange channel WGs on RTP have been reported [18]. Cs^+ ions were used for the exchange process because they produce an increase in the refractive index and its ionic radius is similar to the radius of Rb^+. Up to now, no exchange on (Yb,Nb) doped RTP epitaxial layer has been described. It is known that the doping with Nb^{5+} increases the ionic conductivity in KTP [19] due to the increase of vacancies at the K^+ sites. Also in RTP, Nb^{5+} doping increases the ionic conductivity. However, the doping couple (Yb,Nb) doesn't change the ionic conductivity along the ***c*** direction in comparison with RTP, but interestingly it increases significantly the ionic conductivity along ***a*** crystallographic direction [17], so the (Yb,Nb) codoping is not expected to favor the unidirectional exchange process.

The motivation of the current work is to demonstrate the Cs^+ exchange process for fabricating integrated optic devices such as Y-splitters and Mach-Zehnder structures (MZ) on RTP (001) substrates and (Yb,Nb):RTP epitaxial layers, and to optically characterize the WG structures obtained.

2. Experimental section

Substrate growth: RTP single crystals were grown by applying the Top Seeded Solution Growth-Slow Cooling (TSSG-SC) technique [20]. A vertical tubular single zone furnace was used in all growths experiments. The solution weighed around 200 g and its composition was Rb_2O-P_2O_5-TiO_2-WO_3 = 44.24-18.96-16.8-20 (mol %), located into the RTP primary crystallization region in solutions with 20 mol % WO_3 [21]. The WO_3 has been introduced in the solution to decrease its viscosity and thus favors the crystal growth. The starting precursors were Rb_2CO_3 (99%), $NH_4H_2PO_4$ (99%), TiO_2 (99%) and WO_3 (99%). The homogenization of the solution was performed at 50 K above the expected saturation temperature for a few hours. The saturation temperature was determined by measuring the apparent no growth/no dissolution in a ***c***-oriented-seed RTP crystal in contact with the center of the solution surface with a micrometer. The saturation temperature of the above RTP solution composition is around 1163 K. Supersaturation was created by applying a slow cooling rate of 0.1 K/h for the first 15 K and then 0.05 K/h for the next 10-20 K. Rotation was applied to the crystal, starting at 60 rpm in the initial steps of growth and as the crystal was growing, the rotation was decreased progressively to 40 rpm in order try to maintain the

#234556 - $15.00 USD Received 12 Feb 2015; revised 10 Apr 2015; accepted 11 Apr 2015; published 22 Apr 2015

convection pattern. In several experiments, when the crystal dimension in the (001) plane was enough, a pulling rate of 1 mm per day was applied in order to increase the crystal dimension along the ***c*** direction. When the crystal was fully grown, it was slowly extracted from the solution and maintained slightly above the solution surface while cooled at 30-40 K/h to room temperature. The crystals obtained were colorless and transparent, without macroscopic defects and with well-defined morphology as can be seen in the Fig. 1. Substrates of 1.5 mm thickness were cut from RTP single crystals as plates parallel to the (001) plane and then polished resulting in an average surface roughness of 15 nm.

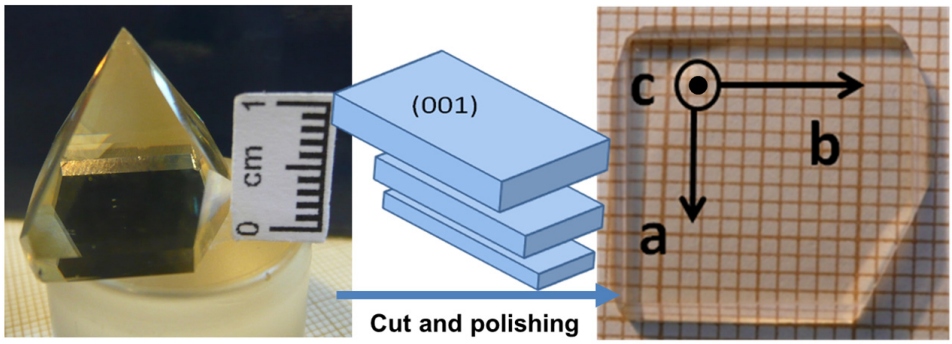

Fig. 1. RTP bulk single crystal grown by TSSG-SC and a cut and polished RTP(001) oriented substrate.

Epitaxial layer fabrication: Epitaxial layers of (Yb,Nb):RTP/RTP(001) were grown by liquid phase epitaxy (LPE) [22]. The solution composition used for LPE experiments was Rb_2O-P_2O_5-TiO_2-Nb_2O_5-Yb_2O_3-WO_3 = 43.9-23.6-20.7-0.45-1.35-10 (mol %). The reagents used were the same as in the growth of substrates, additionally, Yb_2O_3 (99.9%) and Nb_2O_5 (99.9%) were used for doping. Cylindrical crucibles of 25 cm^3 were filled with about 95 g of solution. A well-isolated vertical cylindrical furnace was used, and the crucible was located in a central region of the furnace to obtain a zero vertical thermal gradient in the solution. The solution was homogenized by maintaining at temperatures above the saturation temperature and the determination of the saturation temperature was performed as described above for bulk crystal growth. The RTP(001) substrates were cleaned before introducing them into the solution, which involved the immersion of the substrate in a mixture of HNO_3/H_2O at a 50/50 ratio by volume for 5 min, followed by dipping in distilled water (5 min), then in acetone (5 min) and finally in ethanol (5 min) with a rotation of 60 rpm. After that, the substrates were slowly introduced into the furnace using a stepper motor drive to avoid thermal shocks. Before dipping the substrate into the solution, it was held at a few mm above the surface of the solution for at least 1 h in order to obtain thermal equilibrium between the solution and the substrate. Then, the substrate was dipped into the solution at a temperature of 1 K above the saturation temperature for 5 min in order to dissolve the outer layer of the substrate. Super saturation was created by decreasing the temperature 3 K below the saturation temperature, also rotating at 60 rpm. The growth temperatures were around 1045 K. After 3 h of growth, the sample was extracted very slowly from the solution and held a few mm above it, while the furnace was cooled down to room temperature at a rate of 25 K/h.

Waveguide pattern design: The designs of the waveguide patterns are shown in Fig. 2. The first consists in a symmetric single mode Mach-Zehnder (MZ) design (Fig. 2(a)) without any geometrical path length difference between the two arms and with two identical symmetric Y-structures, the first one acting as a splitter and the second one acting as a combiner. The Y–junction design is based on an S-line pattern, to give low bending losses and a large enough separation between the two arms to minimize the evanescent coupling between the two branches. The long length of the branches is desired for incorporation of

#234556 - $15.00 USD Received 12 Feb 2015; revised 10 Apr 2015; accepted 11 Apr 2015; published 22 Apr 2015

electrodes for electro-optic modulation. 9 mm length MZ structures with radius of curvature ranging from 50 to 80 mm were designed. Figure 2(b), shows the bent WG design based on the same parameters as that of MZ, intended to give additional information on the losses in the MZ waveguide bends. The set of MZs were designed with a length of 9 mm with a separation of 38-42 μm between two arms which gives evanescent coupling free propagation and large radius of curvature provides smooth bend for minimum bending losses. Figure 2(c), shows a straight WG design included in the photolithographic mask to aid alignment and troubleshooting. The width, *w*, of the channels has been fixed to 6 μm. The geometrical parameters of the designs are given in Table 1.

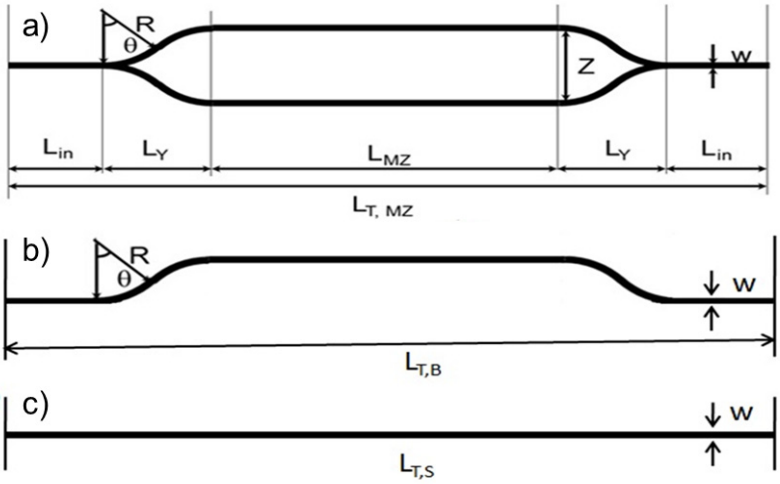

Fig. 2. Pattern design of (a) MZ, (b) S-bend WG, (c) straight WG.

Table 1. Geometrical parameters of the designs.

	L_{in}	L_Y	L_{MZ}	$L_{T,MZ}$	Z	R	$L_{T,B}$	$L_{T,S}$
Dimensions [μm]	1000	2000	3000	9000	38-42	50,000-80,000	9000	9000

Mask preparation: In order to fabricate a dark field mask, a commercially available glass plate coated with chromium and photoresist was used and designs were written on the photoresist with the help of laser lithography. After developing the exposed parts, the designs were transferred on the Cr mask by etching it with commercially available MS8 chrome etchant. This dark field mask in turn was used to transfer the patterns on the RTP samples. This mask contains the patterns of straight WGs, S-bend WGs and MZs. For the preparation of a hard mask on the RTP samples, a 200 nm-thick Ti layer was sputtered onto the RTP at a rate of 0.7 Å/sec with DC power of 200 W using an AJA sputtering system. A layer of photoresist (AZ 1505 from Microchemicals) was then spin-coated onto the Ti-RTP sample and designs were transferred into the resist by using the dark field mask described above using conventional photolithography on an MG 1410 mask aligner. After developing the exposed parts, the designs were transferred into the Ti mask by etching with H_2O_2:NH_4OH in a 2:1 molar ratio.

Ion exchange process: The ion exchange process was conducted in a vertical tubular single zone furnace. The crucible filled with $CsNO_3$ was placed in the furnace where the temperature gradient was almost zero. The sample was previously heated in the furnace to obtain the thermal equilibrium with the melt and then immersed to a depth of 6 mm depth (the

#234556 - $15.00 USD Received 12 Feb 2015; revised 10 Apr 2015; accepted 11 Apr 2015; published 22 Apr 2015

plane of the sample is parallel to the surface of the solution horizontally) in a $CsNO_3$ salt melt maintained at 698 K for 2 h and rotated at 40 rpm in order to obtain a good homogeneity in the liquid. Finally, the sample was slowly extracted from the melt and cooled down at 25 K/h in order to avoid thermal stress. Provided that the ion exchange processing temperature remains at 698 K, the exchange process does not introduce any detectable surface defects. The steps for the sample fabrication process are shown in Fig. 3.

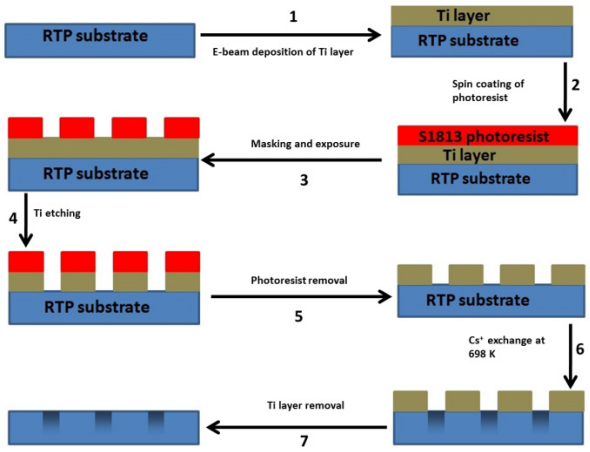

Fig. 3. Steps for the fabrication of the Cs^+ ion exchange WGs in RTP.

In this work, Cs^+-exchange RTP WGs were fabricated along three different crystallographic directions (see Table 2). For future applications in second harmonic generation doubling (SHG) in RTP and self-frequency doubling (SFD) in Yb-doped RTP, the straight channel WG propagation directions were chosen to be parallel to the direction of type II ($e^{\omega} + o^{\omega} \rightarrow e^{2\omega}$) phase matching for 1.05 µm wavelength. These directions are parallel to the [180] direction in RTP ($\theta = 90°$, $\varphi = 76°$) and along [120] direction ($\theta = 90°$, $\varphi = 45°$) in (Yb,Nb):RTP as described in ref [23]. On a second RTP sample, the straight, S-bend and MZ WGs were fabricated along the ***b*** crystallographic direction, in which the sample had the longest dimension. All the samples were fabricated under the same conditions. Table 2 summarizes the description of the fabricated WGs.

Table 2. Description of the fabricated WGs.

Sample	WG [uvw] propagation direction	WG types
RTP(001)	***b***	Straight, S-bend, MZ
(Yb,Nb):RTP/RTP(001)	[120]	Straight WG
RTP(001)	[180]*	Straight WG

*the angle between the ***a*** and [180] is 76°.

Modal characterization: The end faces perpendicular to the channels were polished in the three different samples, to image the near field intensity distribution of the guided modes. A 20X microscope objective (NA = 0.4) was used to couple the light into the input side of the devices and images were collected with a visible camera through a 20X microscope output objective (NA = 0.4). Straight WGs fabricated along the [180] direction were characterized at three different wavelengths: 633, 1064 and 1520 nm using HeNe and diode lasers.

Loss evaluation: In order to estimate the propagation losses of the channel WGs, the fundamental mode was excited in the channel using an x-y-z stage. A 20X microscope objective was used to collect the transmitted light. The beam power was measured before the input microscope objective as well as after the output microscope objective. The expression

#234556 - $15.00 USD Received 12 Feb 2015; revised 10 Apr 2015; accepted 11 Apr 2015; published 22 Apr 2015

applied to estimate the total insertion losses, L_I, was the corresponding to the single pass transmission method,

$$L_I = -10 * \log_{10}\left(P_{wg} / P_{no-wg}\right), \quad (1)$$

Where P_{wg} is the power measured after the output microscope objective with the WG inserted, and $P_{no\text{-}wg}$ is the power measured with both input and output objectives aligned but without the WG. The Fresnel losses L_{Fr}, coupling losses L_C, and the propagation losses L_{Prop}, are the terms whose summation is assumed to give the total transmission insertion losses, $L_I = L_{Fr} + L_C + L_{Prop}$. Coupling losses were evaluated by calculating the overlapping integral of WG output modes and input objective focal spot intensity distributions.

3. Results and discussion

RTP bulk crystal domain map: We have studied the ferroelectric domain structures in an RTP bulk single crystal. The variety of the domain boundaries depends directly on the growth sector number, the kinetics of growth of them, and then directly from the growth method and composition of the flux used for growth [15]; so the description here is for the crystals grown as described before. Two single crystals have been cut in slices perpendicular to the ***c*** crystallographic direction; the resulting plates have been submitted to selective chemical etching in a 2:1 (mol ratio) solution of KOH: KNO_3 for 30 min at 353 K to visualize the domains. It is known that molten salts containing hydroxide attack the negative face (c^-), while the positive face is left essentially untouched.

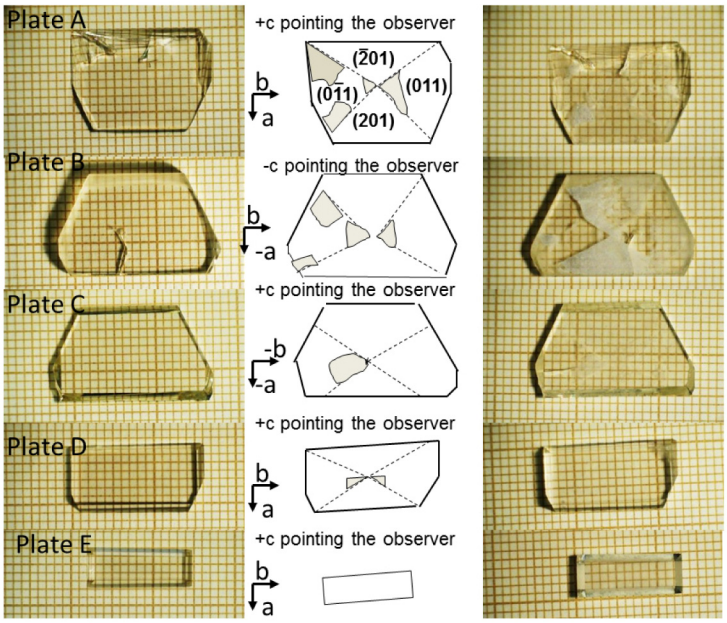

Fig. 4. Cut and polished plates of RTP from a single RTP bulk single crystal, on the left, before the wet chemistry attack, on the right after the wet chemical attack. The attacked parts have been highlighted to help to visualize them.

Roth [15] reported the growth sectors present in KTP and RTP crystals. As can be seen in Fig. 4, mainly in the plates perpendicular to ***c*** direction, there are four main growth sectors, displayed and labelled trough the developed faces in the morphology, the {201} and the {011} sectors, as observed before [24]. In KTP it has been reported that these two sectors are usually mono domain; however as can be observed in Fig. 4, it seems that in RTP the {201} has grown as mono domain, but the {011} sector is multi domain. The domain present in the

#234556 - $15.00 USD Received 12 Feb 2015; revised 10 Apr 2015; accepted 11 Apr 2015; published 22 Apr 2015

{201} sector has a domain boundary coincident with the edge boundary of the growth sector, and can be labelled as a full-size edge; but the small domains with irregular shape located inside the {011} growth sector, they present intra-sector domain boundaries dispersed type [15].

As no reversal domain technique has been applied to our RTP (001) cut samples, it can be predicted that along the diffused channel parallel to the ***b*** crystallographic direction and [180] direction, there can be different ion exchange behavior, because more probably the channel is travelling along different ferroelectric domains.

The epitaxial doped samples are also grown over the Curie temperature (it is expected that the T_c is decreased with the presence of Nb^{5+} [25]), so they are grown as paraelectric samples and no transfer of the domain structure of the substrate can be done [26]. In these samples, the transition from paraelectric phase to ferroelectric phase is done through the cooling period. In this case, as the samples are grown by LPE method on the (001) face, which is not a natural face, a ferroelectric multi domain is also expected [26]. Figure 5 shows an epitaxial sample after the wet etching. As can be observed, it is multi domain, as expected.

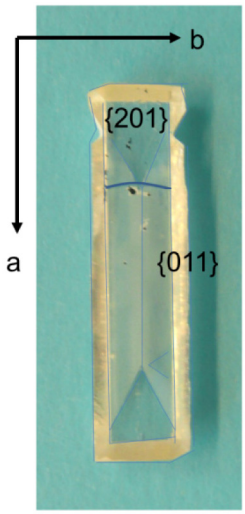

Fig. 5. (Yb,Nb):RTP/RTP(001) epitaxial layer after wet etching.

Ion exchange results: The exchange of Cs^+ as a function of the depth in the RTP samples was measured by electron probe microanalysis (EPMA) with a JEOL JXA-8230 electron microprobe instrument in the wavelength dispersive mode. The accelerating voltage was 15 kV and the beam current 20 nA. The standards used were RTP for Rb, Ti, P and O measurements and CsI for Cs measurement. The analyses were made using the Lα X-ray lines for Rb^+ and Cs^+ and Kα lines for Ti, P and O. The measurements of Rb, Ti, P and O were performed for duration of 10 s and for 30 s in the case of Cs^+. The matrix effect was corrected using the CITZAF procedure.

Figure 6 shows the Cs^+ concentration in weight per cent as a function of the distance from the crystal surface in three different channels in the RTP and two other channels in a (Yb,Nb):RTP epitaxial layer. As can be observed there's no reproducibility of the exchange in the different channels, which may be due to each channel being located in a different crystal growth sector, and then, different ferroelectric domains. It can be also observed that the quantity of Cs^+ introduced in RTP is larger than in the doped (Yb,Nb):RTP. This may be expected due to the similar or lower ionic conductivity when RTP is doped with Yb and Nb [17]. In Gavaldà *et al.* [17], the Nb content of the sample was larger than in the epitaxial sample reported in this work, and the ytterbium concentration was similar; and it was

#234556 - $15.00 USD Received 12 Feb 2015; revised 10 Apr 2015; accepted 11 Apr 2015; published 22 Apr 2015

observed that the couple (Yb,Nb) has similar ionic conductivity than RTP along ***c***, but when compared with single doped Nb samples, the codoping (Yb,Nb) decreases the ionic conductivity along ***c***, so the tendency observed in our samples, is in agreement with the reported tendency of the ionic conductivity. Generally, the Cs^+ concentration decreases with depth and the exchange region is as minimum 6-7 μm.

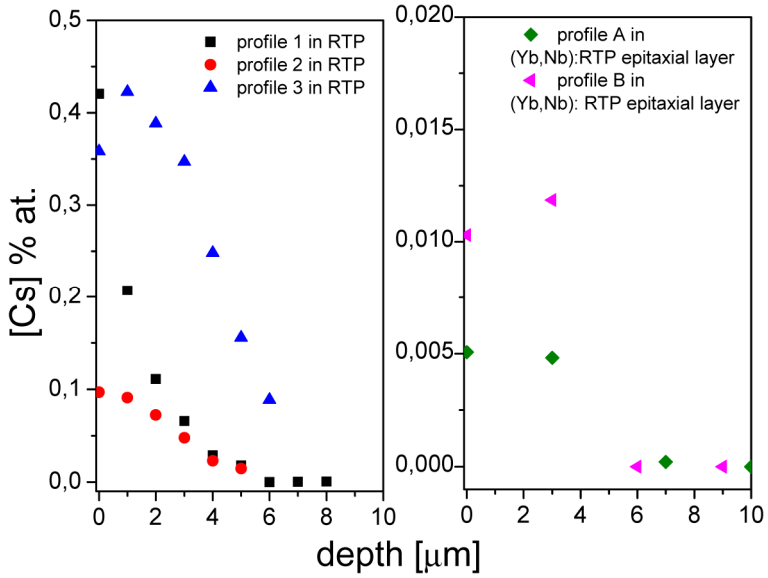

Fig. 6. Cs^+ concentration in the channel as a function of the depth in the RTP substrate and (Yb,Nb):RTP epitaxial layer.

To determine the width of the exchanged channels, we observe the channels by ESEM, after the exchange process. Figure 7 shows the ESEM images. It can be observed that Ti mask layer was removed from the edges of the WG allowing the Cs^+ ions to diffuse in these parts which in turn forms a wider dimension of WG than expected. It can also be seen that the part of the substrate which was directly exposed to the melt shows some chemical etching effects. These inhomogeneities in the channel width along the WG can scatter when light propagates along it.

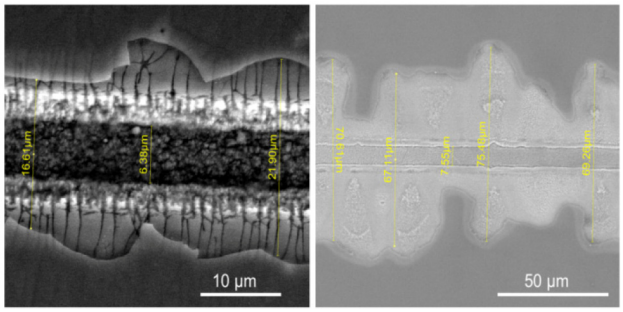

Fig. 7. ESEM images of the top view of (a) Cs:RTP(001) coated with a patterned Ti layer (b) Cs:(Yb,Nb):RTP/RTP (001) sample coated with a patterned Ti layer.

Modal characterization in bulk RTP(001) samples: In the straight, S-bend and MZ WGs realized in RTP(001), light at a wavelength of 633 nm was only guided in the TM polarization. Figure 8(a), shows the mode intensity profile of the guided light in a straight WG with mode field diameters (MFD, at $1/e^2$ intensity) of 43 μm x 22 μm for the horizontal

#234556 - $15.00 USD Received 12 Feb 2015; revised 10 Apr 2015; accepted 11 Apr 2015; published 22 Apr 2015

and vertical profiles, respectively. Figure 8(b) shows a profile for the guided light in an S-bend WG with mode field diameter (MFD) dimensions of 33 µm x 18 µm for the horizontal and vertical profiles, respectively. Figure 8(c) shows a profile of a MZ output with a MFD of 52 µm x 26 µm of horizontal and vertical profiles, respectively. In the same sample straight, S-bend and MZ WGs were measured; in the WGs it was only possible to observe guiding in the TM configuration at 633 nm.

The MFD were in the range from 30 to 50 µm in the horizontal and 20-25 µm in the vertical directions, respectively. A correlation can be found between the horizontal dimension of the WG with the sizes of the mode in horizontal dimension, observing at the ESEM images of the "diffused region" (as an example see Fig. 7). In previous work where the Cs^+ exchange was also done in a channel along the ***b*** direction in a RTP (001) substrate with the same experimental conditions [18], the size of the modes for guided light at 633 nm, was 9.7µm x 7.5 µm, horizontal and vertical dimensions, respectively, despite the observed exchange depth being around 20 µm.

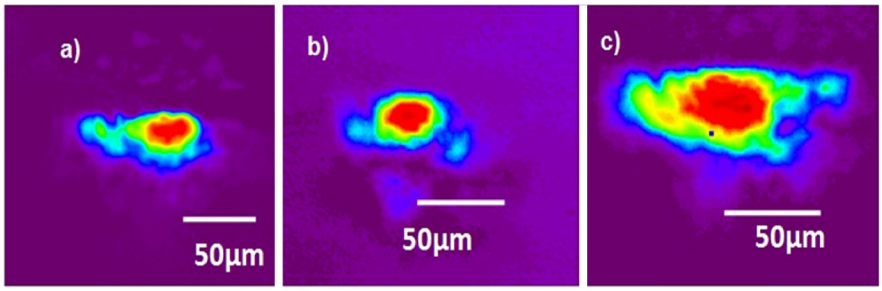

Fig. 8. (a) Near field mode intensity profile from a 9 mm long straight WG, (b) of the output guided modes in a 9 mm long S-bend WG, (c) of the output guided mode in 9 mm long MZ at 633 nm.

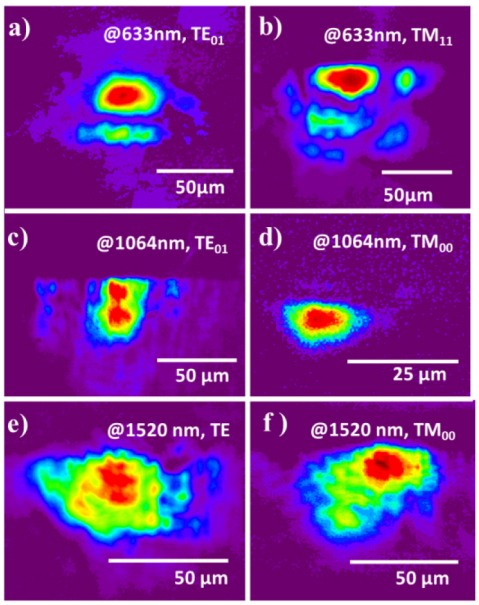

Fig. 9. (a) Near field image of the TE_{01} mode at 633 nm of a straight WG, (b) Near field image of TM_{11} mode at 633 nm of a straight WG, (c) Near field image of the TE_{01} at 1064 nm of a straight WG, (d) measured near field image of the TM_{00} at 1064 nm of a straight WG, (e) Near field image of the TE mode at 1520 nm of a straight WG, (f) Near field image of the TM_{00} mode at 1520 nm of a straight WG.

#234556 - $15.00 USD Received 12 Feb 2015; revised 10 Apr 2015; accepted 11 Apr 2015; published 22 Apr 2015

It can be observed that almost all the WGs are multimode and support more modes at shorter wavelengths as expected. The successful guidance in both polarizations may allow the generation of SHG by type II configuration in future applications. Comparing the WGs fabricated in RTP along ***b*** and along [180], we can highlight that the guided modes are not similar, due to the different index contrast produced by the different Cs^+ concentration profiles. Further, for this last sample, we have observed the TE_{01} and TM_{11} modes at 633 nm, which means that this WG can support at least 2 TE modes and 4 TM modes indicating that $\Delta n_{(001)plane} << \Delta n_z$. In previous works, Bierlein and Vanherzeele (1989) [11], in the WG fabricated by ion exchange in KTP, reported that the obtained Δn was isotropic ($\Delta n_x = \Delta n_y = \Delta n_z$), however later Buritskii *et al.* [27,28] determined that in the case of Rb^+ diffused KTP WG, the $\Delta n_x \sim 2\ \Delta n_z$.

Modal characterization in epitaxial (Yb, Nb) doped RTP samples: Straight WGs were fabricated by Cs^+ exchange on (Yb,Nb) doped epitaxial sample RTP in order to examine the effect of (Yb, Nb) doping ions on Cs^+ exchange. Cs:(Yb,Nb):RTP/RTP(001) straight WGs fabricated along [120] were characterized as described above at 633 nm. In this case light was only confined and guided in the TM polarization. The near -field mode intensity profiles of a straight WG are shown in Fig. 10.

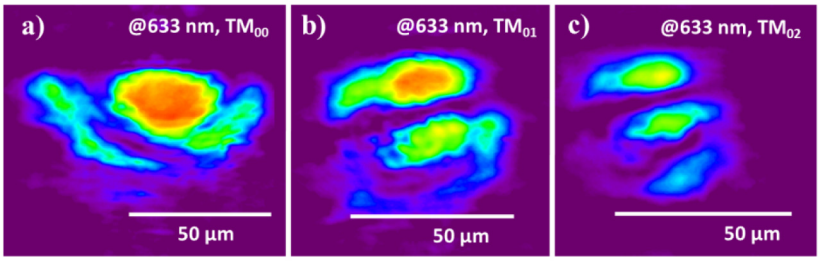

Fig. 10. TM modes of straight WGs fabricated on Cs^+ exchanged (Yb,Nb):RTP/RTP(001) along the [120] direction.

When comparing the guiding properties of the Cs^+ exchanged sample in RTP with that in the (Yb,Nb):RTP, it can be inferred that there is a larger refractive index contrast in the RTP samples (in agreement with the EPMA measurements), in which guiding has been observed in both polarizations, TE and TM; also the TM_{11} mode has been observed, implying that the waveguide supports a minimum of 5 modes.

Table 3. Losses evaluation in Cs^+ exchanged WGs.

Sample	λ [nm]	Pol.	WG	[uvw]	L_C [dB]	L_{Fr} [dB]	L_I [dB]	L_{Prop} [dB/cm]
RTP(001)	633	TM	Straight	***b***	10.0	0.9	22.6	11.3
	633	TM	S-Bend	***b***	8.1	0.9	23.4	15.8
	633	TM	MZ	***b***	11.5	0.9	21.7	10.4
	633	TE	Straight	[180]	7.5	0.7	14.5	5.7
	633	TM	Straight	[180]	7.0	0.7	25.2	15.9
	1064	TE	Straight	[180]	5.9	0.7	27.3	18.8
	1064	TM	Straight	[180]	1.4	0.7	30.9	26.1
	1520	TE	Straight	[180]	11.4	0.7	19.3	6.6
	1520	**TM**	**Straight**	**[180]**	**10.6**	**0.7**	**16.8**	**5.0**
(Yb,Nb):RTP/RTP(001)	633	TM	Straight	[120]	2.8	0.9	21.8	15.5

#234556 - $15.00 USD Received 12 Feb 2015; revised 10 Apr 2015; accepted 11 Apr 2015; published 22 Apr 2015

Loss calculation of the samples: Using the expression (1), we estimated an upper limit on the propagation losses of the measured TM and TE guided modes. For the sample with all designs, we have evaluated the total losses, and they are summarized in Table 3. In all WGs, propagation losses are around 15-30 dB, rather large. The contribution to the total losses due to the S-bend and Y-splitter cannot be distinguished due to the large deviation in the loss measurements. As described above, the waveguide width varies strongly along the waveguides, due to the different ferroelectric domains along the WG and the over etching of the Ti masks, resulting in these rather high losses and large variation of values. These values are larger than previous reported values, published by Choudhary *et al.* [9], in channel WGs fabricated by RIE in RTP(001) bulk samples, in which the transmission losses were around <3.5 dB/cm at 980 nm.

Conclusions

In summary, waveguides based on Cs^+ exchange in $RbTiOPO_4$(001) and (Yb,Nb):$RbTiOPO_4$ have been fabricated in different configurations: straight, S-bend and MZs. The Cs^+ exchange profiles achieved are not reproducible in a single sample due to the presence of different ferroelectric domains. The Cs^+ exchange is favored in the undoped RTP(001) samples when compared with doped epitaxial (Yb,Nb):$RbTiOPO_4$/RTP(001). All waveguides confined light, with the observed near field mode intensity distributions larger than expected, taking into account the measured diffused region. High total losses were obtained due to scattering and microbending effects generated by the inhomogeneities along the Cs^+ exchanged region. To reduce the observed losses, the over etching of the Titanium mask could be reduced using shorter etching times or changing the metal used for the hard mask to obtain a better control of the Cs^+ exchange regions. Further studies would be needed to modify the ferroelectric domain distribution in the grown single crystals.

Acknowledgments

This work was supported by the Spanish Government under Projects MAT2011-29255-C02-02, TEC2014-55948-R, and MAT2013-47395-C4-4-R/1-R, by the Catalan Authority under Project 2014SGR1358. F. D. acknowledges additional support through the ICREA academia award for excellence in research. M. Ali Butt thanks the Catalan Government for the FI-DGR fellowship 2012FI-B 00192.